



Universiteit
Leiden
The Netherlands

Rare-earth nanoparticles in bioimaging and therapy

Yu, Z.

Citation

Yu, Z. (2023, July 5). *Rare-earth nanoparticles in bioimaging and therapy*. Retrieved from <https://hdl.handle.net/1887/3629783>


Version: Publisher's Version

License: [Licence agreement concerning inclusion of doctoral thesis in the Institutional Repository of the University of Leiden](#)


Downloaded from: <https://hdl.handle.net/1887/3629783>

Note: To cite this publication please use the final published version (if applicable).





Recent advances in rare-earth-doped nanoparticles for NIR-II imaging and cancer theranostics



This chapter was adapted from "Yu, Z., Eich, C., & Cruz, L. J. (2020). *Frontiers in Chemistry*, 8, 496."

Abstract:

Fluorescence imaging in the second near infrared window (NIR-II, 1000-1700 nm) has been widely used in cancer diagnosis and treatment due to its high spatial resolution and deep tissue penetration depths. In this work, recent advances in rare-earth-doped nanoparticles (RENPs) - a novel kind of NIR-II nanoprobes - are presented. The main focus of this study is on the modification of RENPs and their applications in NIR-II *in vitro* and *in vivo* imaging and cancer theranostics. Finally, the perspectives and challenges of NIR-II RENPs are discussed.

1 Introduction

Cancer is one of the world's most lethal diseases, and there are no particularly effective treatments to date. Cancer patients must endure chemotherapy and radiotherapy, followed by long-term medications, which are a great burden on their body and mind. For people not to be afflicted by cancer, it is necessary to diagnose the disease in an early stage and personalize treatments based on each patient's individual variability and medical profile[1]. Molecular imaging modalities can be useful for the comprehensive evaluation of essential biomolecules and can facilitate the non-invasive visualization of cell function and biochemical processes in biological systems[2-4]. They are well recognized as powerful techniques that provide more comprehensive anatomical, physiological and functional information in early cancer detection, drug delivery, as well as monitoring treatment effectiveness[5-7]. Currently, varieties of molecular imaging techniques are widely used in the medical field, including magnetic resonance imaging (MRI), X-ray computed tomography (CT), positron emission tomography (PET), single-photon emission computed tomography (SPECT) and optical fluorescent light imaging (FLI) (Fig. 1). However, these methods have some disadvantages. For example, CT and MRI often require high doses of contrast agents; PET and SPECT require radioactive tracers that can put both patients and operators in danger[8-11]. Also, they need to be optimized to obtain more accurate information due to their long scanning time and low sensitivity/spatial resolution[12, 13].

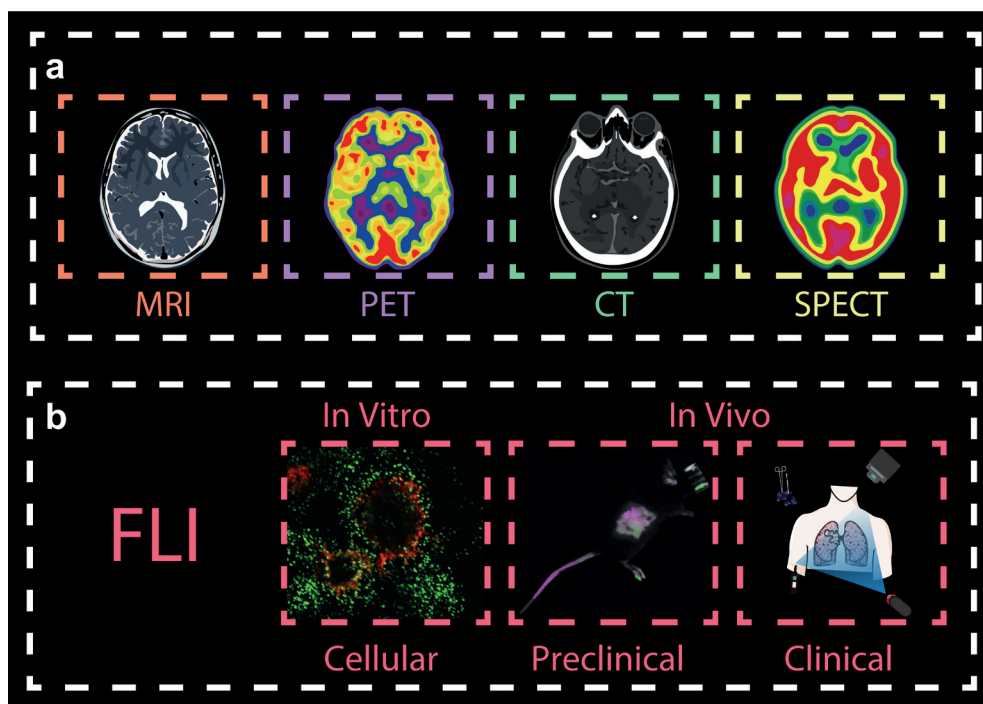


Figure 1 Overview molecular imaging techniques. The main imaging methods are (a) magnetic resonance imaging (MRI), X-ray computed tomography (CT), positron emission tomography (PET), single-photon emission computed tomography (SPECT) and (b) optical fluorescent light imaging (FLI). While MRI, PET, CT and SPECT are widely used in the clinics, FLI techniques are mainly used in biomedical preclinical research *in vitro* and *in vivo*, with the exception of fluorescence image-guided surgery, a medical imaging technique used to detect fluorescently labelled structures during surgery. This review, we will focus on introducing FLI from both *in vitro* and *in vivo* imaging.

In recent years, optical imaging has attracted much attention in various fields, predominantly preclinical research because it provides excellent real-time visualization, high sensitivity and spatial resolution, especially in early detection and diagnosis of cancer. Generally, most of the conventional

imaging agents operate in the short-wavelength region (e.g., the ultraviolet (UV) and visible regions). In these regions, light signals are easily absorbed and scattered by certain biological tissues (such as muscle, skin and body fluids). This leads to high autofluorescence, low signal-to-background ratio and low tissue penetration[14, 15]. Besides, high-energy light can lead to photo-toxicity damage in biological tissues. To circumvent these problems, optical imaging in the near-infrared (NIR) region, which is located in the so-called “biological window”, has gained much attention (Fig. 2). Imaging agents in the first near-infrared window (NIR-I, 700-900 nm) are gradually being known by researchers, and can provide deep and sensitive bioimaging. However, their limited tissue penetration depth (less to 1 cm) and large photon scattering losses in biological samples still restrict their use further in biomedical diagnosis and therapy. To address these challenges, novel materials that enable fluorescent imaging in the NIR-II window (1000-1700 nm) for biomedical applications have been developed. They show better resolution because they have deeper penetration (~1.8 cm) and lower autofluorescence. Therefore, there is need to synthesize the novel NIR-II agents with high efficiency and resolution for biological imaging application[16].

So far, many types of fluorescent agents with emission in the NIR-II region have been extensively applied for effective bio-sensing and real-time *in vitro* and *in vivo* imaging of living species (Fig. 2). They include single-walled carbon nanotubes (SWNTs)[17, 18], organic dyes[19, 20], conjugated polymers[21], quantum dots (QDs)[22], gold nanorods[23, 24] and rare-earth-doped nanoparticles (RENPs)[25, 26]. However, most of them have some disadvantages, such as the broad emission bandwidths of SWNTs, short accumulation time of organic dyes, high toxicity, low quantum yield and low solubility of QDs. These disadvantages will vastly inhibit their further applications in NIR-II imaging. RENPs are good candidates for NIR-II optical imaging, because they show minimal photo-bleaching, superior luminescent lifetimes, excellent tunable emission wavelengths and low

biotoxicity[27-32].

Rare earth elements constitute a class of lanthanide ions found in the 6th row of the periodic table (La, Ce, Pr, Nd, Pm, Sm, Eu, Gd, Tb, Dy, Ho, Er, Tm, Yb, Lu), as well as two other elements closely related to the lanthanides - yttrium (Y) and scandium (Sc). Due to the incompletely filled 4f shell and the spin-orbital coupling of 4f free ions, they possess extremely complex optical properties. One of the most interesting features of these ions is their photoluminescence. The luminescence of the trivalent lanthanide ions arises from f-f transitions of the 4f shell and f-d transitions in the 4f-5d shell. The f-f transitions also provide the lanthanide elements with rich energy level structures in the UV, VIS and NIR ranges. As they can be tuned from the UV to the NIR region, most nanomaterials made of rare-earth elements can be classified into two major categories: Upconversion nanoparticles (UCNPs) and downconversion nanoparticles (DCNPs). DCNPs can downconvert a high energy photon into two or more low-energy photons. In contrast, UCNPs can convert long-wavelength light (low energy) to short wavelength (high energy). Unfortunately, due to the unique anti-Stokes optical properties of UCNPs, most of the NIR-II nanoprobe belong to the category of DCNPs. Until now, a large number of studies have shown that by using suitable sensitizers, UCNPs can obtain longer excitation wavelength for NIR-II imaging[33]. For example, emissions in the NIR-II region of Ho³⁺ and Nd³⁺ could be obtained from Er³⁺ sensitized UCNPs[34].

Based on the excellent characteristics of rare-earth ions, such as their low photobleaching, various absorption and emission wavelengths, and low energy losses, NIR light-mediated RENPs have been widely used in *in vitro* and *in vivo* imaging of biomolecules. Commonly, this kind of downconverting nanoparticle combines rare-earth ions and an inorganic crystalline host lattice (e.g. NaYF₄, NaLuF₄ and CaF₂). The host can also provide an environment for energy transfer from a sensitizer to a rare-earth dopant resulting in NIR-II fluorescence.

This review mainly introduces the recent advances in RENPs fluorescent imaging in the NIR-II region. In particular, we focus on the modification of these nanoparticles by lipids or dyes, and their use in cancer diagnosis and therapy. Then, the challenges and prospects of RENPs are discussed.

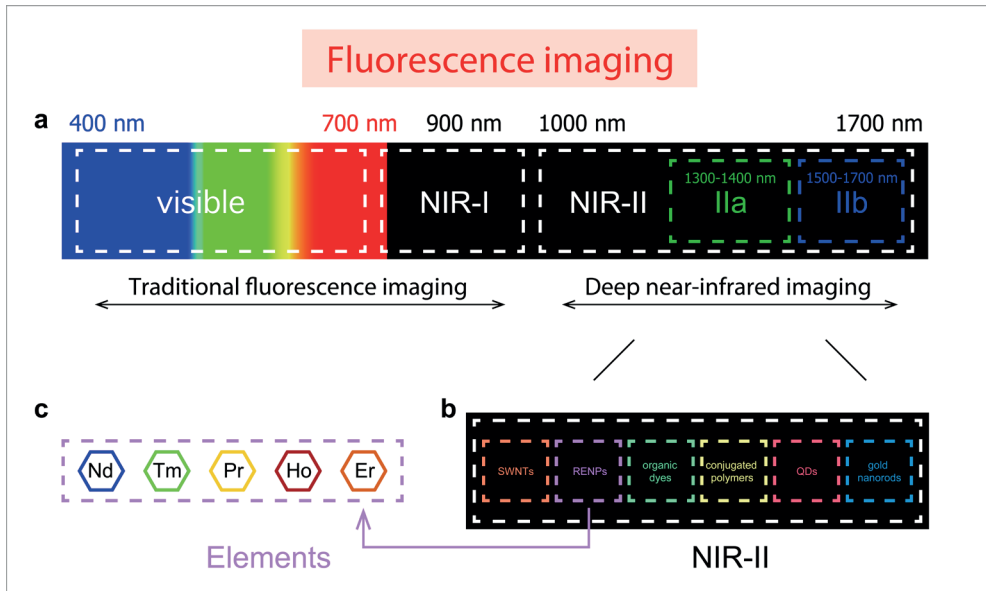


Figure 2 Spectral overview fluorescence imaging techniques. (a) Spectral ranges of traditional fluorescence imaging techniques, including the near-infrared (NIR)-I region, and the deep NIR-II region. (b) Imaging probes commonly used in the NIR-II region: Single walled nanotubes (SWNTs), rare-earth-doped nanoparticles (RENPs), organic dyes, conjugated polymers, quantum dots (QDs) and gold nanorods. (c) Neodymium (Nd)-, thulium (Tm)-, praseodymium (Pr)-, holmium (Ho)- and erbium (Er)-containing RENPs have attracted wide attention.

2 Main kinds of RENPs

Based on the energy level of the rare earth elements, most RENPs possess upconversion and downconversion properties. Up to date, thanks to the effort of many researchers, five of them are reported and extensively

explored as activators emitting in NIR-II regions, having excellent downconversion emission (1060/1300 nm for Nd³⁺, 1470 nm for Tm³⁺, 1310 nm for Pr³⁺, 1185 nm for Ho³⁺ and 1525 nm for Er³⁺)[35] (Fig. 2).

2.1 Nd-doped nanoparticles

According to recent studies, Nd³⁺ has gained attention for bioimaging applications due to its special illumination at 808 nm and deep tissue penetration[36]. With strong absorption at 730 nm, 808 nm or 860 nm, Nd³⁺ can transfer photons with the generation of electrons from the ⁴I_{9/2} ground state to the ⁴F_{7/2}, ⁴F_{5/2} or ⁴F_{3/2}; then the electrons move back to the ⁴F_{3/2} state, which can reduce the overheating effect of tissues usually caused by 980 nm light. As a result of the two transitions, the emission corresponds to 1060 nm (⁴F_{3/2}→⁴I_{11/2}) and 1330 nm (⁴F_{3/2}→⁴I_{13/2}) in the NIR-II region. Thus, it provides a good way to avoid autofluorescence of tissue.

Earlier attempts of using Nd-doped nanomaterials as NIR-II biomedical imaging agents have been described[37, 38]. In 2002, Stouwdam *et al.* first realized that Nd³⁺ doped LaF₃ nanoparticles can be utilized as a polymer-based optical component under 514 nm laser excitation[39]. Then, Wang *et al.* developed the synthesized method of LaF₃: Nd³⁺. It was carried out in aqueous solution at low temperature, and showed great NIR-II emission under 802 nm laser excitation[40]. In 2014, LaF₃: Nd³⁺ nanoparticles were used to obtain both *in vitro* and *in vivo* images in cancer cells and mice by Rocha *et al.* The results showed that LaF₃: Nd³⁺ nanoparticles are a very promising fluorescent nanoprobe for bioimaging in the second NIR window[29]. One year later, Villa and his group did an exciting work on high-contrast *in vivo* imaging in the second biological window[37]. This work showed how to produce autofluorescence free, high contrast *in vivo* fluorescence imaging with 1340 nm emission band of SrF₂: Nd³⁺ nanoparticles. They found that autofluorescence of animal diet can extend up to about 1,100 nm, which demonstrated that food-related infrared autofluorescence has an impact on the study of reliable biodistribution.

In the past 3 years, some new host matrices have been reported, such as LiYF_4 [30], GdPO_4 [41], CaTiO_3 [42], and NaDyF_4 [43]. As we know, higher Nd^{3+} doping will result in severe quenching of concentration, so to induce great fluorescence signals, the concentration of Nd^{3+} should be controlled between 1% and 5%. Thanks to intensive research, most of these new Nd^{3+} doped systems are nowadays not only used *in vivo* NIR-II imaging but also in X-ray CT bioimaging or MRI. Due to the large X-ray absorption coefficient of Gd^{3+} , Dy^{3+} , dual-mode molecular imaging has become a new trend in bioimaging, such as NIR-II imaging/CT, NIR-II imaging/MRI, NIR-II imaging/PET.

Despite the efforts made so far as seen above, low optical effects are still a major drawback. However, sensitizers and core-shell structures that can be used to increase the signal-to-noise ratio are gradually becoming more known in the field of NIR-II bioimaging, disease detection and treatment. For example, $\text{NaGdF}_4: \text{Nd}^{3+}, \text{Yb}^{3+}, \text{Tm}^{3+}$ is a novel nanomaterial which uses Gd^{3+} as bridge ions and finally traps energy by the initial activator ions (Nd^{3+})[44]. Other previous studies also showed that co-doping with Y^{3+} can effectively reduce the aggregation of Nd^{3+} in CaF_2 , resulting in a greater luminescence enhancement of Nd^{3+} [38]. Chen *et al.* synthesized high quantum yield core/shell $\text{NaGdF}_4: 3\%\text{Nd}^{3+}@\text{NaGdF}_4$ nanoparticles with an average size of 15 nm. An *in vitro* and *in vivo* NIR-II bioimaging was obtained by loading HeLa cells with $\text{NaGdF}_4: 3\%\text{Nd}^{3+}@\text{NaGdF}_4$ nanoparticles and transferring $\text{NaGdF}_4: 3\%\text{Nd}^{3+}@\text{NaGdF}_4$ nanoparticles in a nude mouse model[45]. CaF_2 was also used as the shell material to make $\text{NaYF}_4: \text{Yb}, \text{Nd}@\text{CaF}_2$ core/shell nanoparticles, which resulted in high contrast multiplexed *in vivo* imaging in the NIR-II region[46]. In 2018, inspired by Chen's work, Wang *et al.* fabricated $\text{NaGdF}_4: 5\%\text{Nd}^{3+}@\text{NaGdF}_4$ by the successive layer-by-layer (SILAR) method. To obtain DCNPs-L1-FSH β nanoprobe via an EDC/NHS reaction, image-guided surgery for metastatic ovarian cancer could be improved. Utilizing these novel nanoprobe, metastases with ≤ 1 mm can be completely resected under the guidance of NIR-II imaging[47]. A

recent report showed that the ultra-small NaGdF₄: 5 %Nd@NaGdF₄ (4.38 ± 0.57 nm) nanoparticles can be applied in the precise inflammation bioimaging by ROS (reactive oxygen species)-responsive cross-linking after modification with GSH (Glu-Cys-Gly)[31, 48]. An interesting work based on supramolecular self assembly strategy is developed for NIR-II imaging assembly and disassembly through NaGdF₄: 10%Y, 25%Yb, 0.5%Tm@NaGdF₄ UCNP@azobenzene and NaGdF₄: 5%Nd@NaGdF₄ DCNP@β-cyclodextrin. The new strategy allows flexible assembly and disassembly of nanoparticles by controlling different near-infrared lasers, which can reduce the background of biological imaging and long-term cytotoxicity, while providing technical support for further accurate image-guided tumor surgery[49]. As only a few NIR-II fluorophores can be used directly for bone imaging without linking to targeted ligands, He *et al.* demonstrated DSPE-mPEG encapsulated with β-phase NaYF₄: 7%Nd@NaYF₄ can be used for bone and vascular imaging, even real-time image-guided lymph node mapping and resection[50] (Table.1).

| NIR-II compositions | Excitation wavelength (nm) | Emission wavelength (nm) | Ligands | Applications |
|---|----------------------------|--------------------------|---------|---|
| SrF ₂ : Nd ³⁺ | 808 | 900-1500 | - | <i>In vitro</i> and <i>in vivo</i> NIR-II imaging |
| CaF ₂ : Y ³⁺ , Nd ³⁺ | 808 | 1058 | - | <i>In vivo</i> NIR-II imaging |
| LaF ₃ : Nd ³⁺ | 808 | 910, 1050, 1330 | - | <i>In vitro</i> and <i>in vivo</i> NIR-II imaging |
| LiYF ₄ : 5%Nd ³⁺ | 808 | 900, 1050, 1330 | EDTMP | Bio-imaging and biodetection |
| GdPO ₄ : Nd ³⁺ | 808 | 1050, 1330 | DOX | Dual-modal <i>in vivo</i> NIR-II/X-ray bioimaging and pH-responsive drug delivery |

| | | | | |
|---|---------|------------|------------------------------------|---|
| NaDyF ₄ : 10%Nd | 808 | 1050, 1330 | Gallic acid-Fe(III) | NIR-II imaging, MRI imaging, PTT |
| NaGdF ₄ : Nd ³⁺ , Yb ³⁺ , Tm ³⁺ | 800 | 980, 1060 | - | NIR-II imaging, MRI imaging |
| NaGdF ₄ : Nd ³⁺ @NaGdF ₄ | 740/900 | 1050, 1300 | - | <i>In vitro</i> and <i>in vivo</i> NIR-II imaging |
| NaYF ₄ : Yb, Nd@CaF ₂ | 808 | 980, 1350 | Poly(acrylic acid) | Lifetime-gated <i>in vivo</i> multiplexed imaging |
| NaGdF ₄ : 5%Nd@NaGdF ₄ | 808 | 1060 | DSPE-PEG-NH ₂ -DNA-FSHβ | Image-guided surgery for metastatic ovarian cancer |
| NaGdF ₄ : 5%Nd@NaGdF ₄ | 808 | - | GSH (Glu-Cys-Gly) | <i>In vivo</i> inflammation Imaging |
| β- NaYF ₄ : 7%Nd@NaYF ₄ | 808 | 1064, 1345 | DSPE-mPEG | NIR-II imaging of bone, vascular tissue and thrombi |

Table 1 Characteristics of Nd-RENPs NIR-II nano-composites.

2.2 Er-doped nanoparticles

With the rapid development of the RENPs, Er³⁺ doped nanoprobe are mainly synthesized as upconversion nanomaterials and applied in the VIS and NIR-I regions. In 2011, Y₂O₃: Yb, Er nanoparticles modified by PEG-b-PVBP and PEG-PO₃H₂ showed NIR emission at 1550 nm in organs of live mice[51]. Then people considered Er³⁺ as a better dopant since it can exhibit strong downconversion luminescence in NIR-IIb region. Nanoprobes employed in the NIR-IIb region are better for bioimaging, owing to their deeper tissue penetration, higher spatial and temporal resolution and lower

autofluorescence than those in the NIR-IIa region; but rare-earth based nanoprobes with high spatial and temporal resolution imaged in NIR-IIb region are still very scarce. There is no doubt that the special characteristic of Er^{3+} solves the main problem that has plagued researchers for a long time. Two years later, Naczynski *et al.* first used $\text{NaYF}_4: \text{Yb}, \text{Ln}$ (Ln: Er, Ho, Tm or Pr) for *in vivo* imaging of tumors. They demonstrated that Er^{3+} doped nanoprobes were the brightest one. Especially, by encapsulating RENPs with albumin, they provided a good method to improve tumour accumulation[52]. Then, Er^{3+} codoped Yb^{3+} nanoprobes have attracted increasing attention due to their special application potential. Polyacrylic acid (PAA) modified $\text{NaYF}_4: \text{Gd}/\text{Yb}/\text{Er}$ nanoprobes have been synthesized and have opened the opportunities for NIR-IIb *in vivo* imaging, non-invasive brain vessel imaging and tiny tumor detection guided by optical imaging[53]. In 2016, Dang *et al.* used the well-established technology, Layer-by-Layer (LbL) to design a NIR-II based theranostic platform by $\text{NaYF}_4: \text{Yb}, \text{Er}$ -PLA/DXS/PLA/HA nanoprobes, which can accumulate in diseased sites and demonstrate diagnostic capabilities within an ovarian tumor mouse model. This study demonstrated that these nanoprobes can serve as a promising theranostic platform to monitor the progression and treatment of serous ovarian cancer[54]. Indeed, core-shell is well known for its unique ability to enhance the Er^{3+} emission at NIR-II region. This special structure does not only delay the degradation of dopant but also decreases the quenching effects and strengthens fluorescence. Simple $\text{NaYF}_4: \text{Yb}/\text{Er}@ \text{NaYF}_4$ nanoprobes have been prepared to realize real-time surveillance of metastatic lesions[55]. Deng *et al.* proposed Sc-based probes ($\text{KSc}_2\text{F}_7: \text{Yb}^{3+}/\text{Er}^{3+}$), which are significantly different from the traditional NaYF_4 host. After modification with PAA, they showed a ~ 1.70 -fold stronger fluorescence than the PAA- NaYF_4 nanocrystals under 980 nm excitation. On this basis, they performed the first case of through-skull fluorescence imaging of brain vessels with $\text{KSc}_2\text{F}_7: \text{Yb}^{3+}/\text{Er}^{3+}$ probes[56]. Normally, Yb^{3+} can transfer energy to Er^{3+} $^4\text{I}_{11/2}$ level to release non-radiative photons to the $^4\text{I}_{13/2}$ level, and then

radiate to the $^4I_{15/2}$ level to produce the 1550 nm downconversion emission. During this process, upconversion and quenching effects will decrease the intensity of Er^{3+} downconversion emission. As an alternative, Ce^{3+} is developed as a doping element in Er-doped nanoparticles to improve the NIR-II downconversion emission by efficiently accelerating non-radiative relaxation of $Er\ ^4I_{11/2} \rightarrow ^4I_{13/2}$. $NaYbF_4: 2\%Er, 2\%Ce@NaYF_4$ nanoparticles have been made to prove Ce^{3+} can highly suppress the upconversion with the downconversion pathway boosted by about 9-fold. This can lead to fast NIR-II cerebral-vasculatures imaging by modified PMF-PEG[57]. The synthesis of $NaCeF_4: Er/Yb@NaCeF_4$ has further verified the efficient energy transfer of $Yb^{3+}-Er^{3+}-Ce^{3+}$. Surface modification with DSPE-PEG2000-COOH proved to be a useful method to detect uric acid and can be a key approach in a physiological survey and clinical diagnosis[58]. Interesting research has been done to design and implant QR codes into a mouse by incorporating $NaYF_4: Tm^{3+}/Er^{3+}@NaYF_4$ into polydimethylsiloxane (PDMS) matrices. The QR code consists of black squares arranged in a square grid on a white background according to certain rules, and the imaging device can read the data from the horizontal and vertical components of the image. It provides a possibility for NIR-II *in vivo* information storage and decoding[59]. A core/multishell structure ($NaGdF_4@NaGdF_4: Yb/Er@NaYF_4: Yb@NaNdF_4: Yb$) has also been used for breast cancer diagnostics *in vivo* [60]. Recent progress has focused on the diversification of Er-doped rare-earth nanoparticles. $NaYF_4: Er$ nanoparticles conjugated with the indocyanine green dye (ICG) have been applied to bioimaging in the NIR-II window because of their high spatial resolution. Due to high absorption cross-section of ICG, excitation efficiency of Er^{3+} is increased by the energy transfer mechanism and has proved the potential of $ICG-NaYF_4: Er$ nanoconjugates for multimodal theranostics[61] (Fig. 3). Since NIR-II imaging-guided photothermal therapy (PTT) is rarely explored, Liu *et al.* have successfully developed a core-shell structured $NaLuF_4: Gd/Yb/Er$ NRs@PDA as a nanoplatform that can simultaneously be used to diagnose and treat tumors. It can not only be

used to realize NIR-II imaging but also to enable image-guided PTT[62].

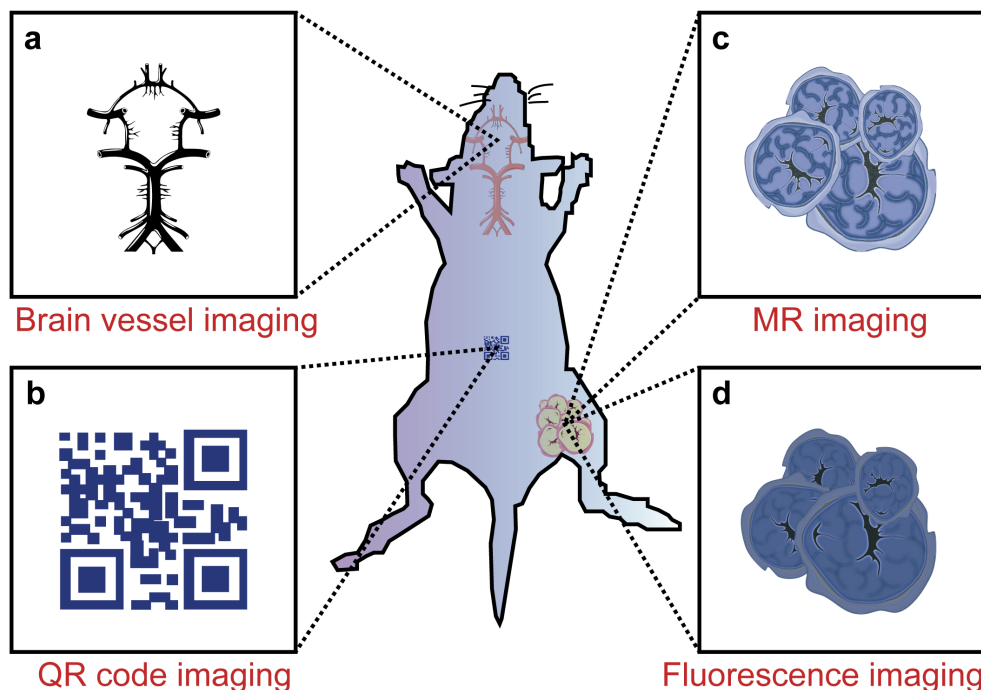


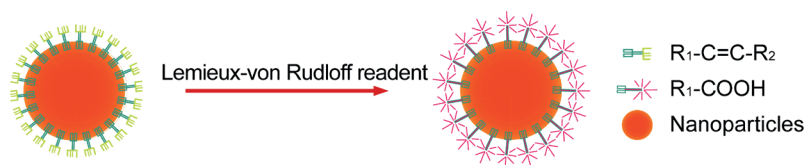
Figure 3 Preclinical application of Er-RENPs in the NIR-II region. (a) NIR-II brain vessel imaging, (b) NIR-II QR code imaging and (c-d) dual mode MRI imaging/ NIR-II fluorescence imaging.

3 Synthesis and modification

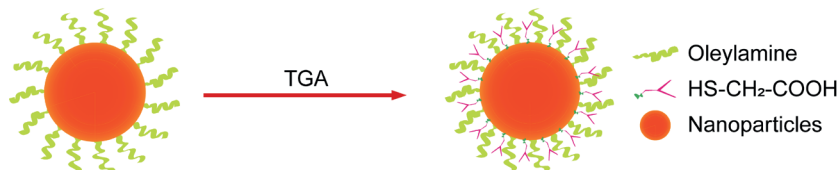
At present, RENPs are synthesized by a solvothermal method, which is technically mature. Solvothermal synthesis is a solution chemistry method that crystallizes nanomaterials of different sizes and morphologies directly from solution under a certain temperature and pressure. To synthesize RENPs with uniform size and morphology, good dispersibility and high luminous efficiency, the size and morphology have to be controlled by adjusting the ratio of raw materials, temperature and solvents[63-68]. On the other hand, because this process cannot precisely control the distribution of dopants, the local relative enrichment of the dopants usually

occurs, resulting in the reduction of luminescent efficiency. In order to avoid the deficiency, one pot successive layer-by-layer (SLBL) strategy is used to synthesize homogeneous doping core (HOC) nanoparticles by growing uniform shells[69, 70]. However, RENPs prepared with oleic acid as reagent are hardly soluble in water and difficult to attach to biomolecules. This limits their application in cell labelling and fluorescent imaging. It is therefore necessary to convert a hydrophobic group into a hydrophilic group by surface modification (for example, $-\text{COOH}$, $-\text{NH}_2$ or $-\text{SH}$). Alternatively, Dong *et al.* have reported the oleate ligands attached to the UCNPs surface can be replaced by nitrosonium tetrafluoroborate (NOBF_4)[71]. Currently, the main surface modification methods used are ligand oxidation, ligand exchange and layer-by-layer self-assembly[72, 73]. The nanoparticle size does not increase after the water-soluble modification using the ligand exchange method, and it is not easy to control the exchange efficiency and effect of water solubility. After using ligand oxidation for modification, due to the shortening of the ligand carbon chain, polar solvent water cannot be effectively suppressed not to quench the fluorescence, and also the fluorescence intensity is much weaker. This method is only suitable for the oxidation of ligands containing carbon-carbon double bonds ($\text{C}=\text{C}$). Therefore, it is still a hot research topic to select effective water-soluble modification methods to obtain RENPs with small particle size, good water solubility and high fluorescence intensity. The following is a brief summary to the currently used surface modification methods (Fig. 4).

a Ligand oxidation



b Ligand exchange



c Layer-by-layer self-assembly method

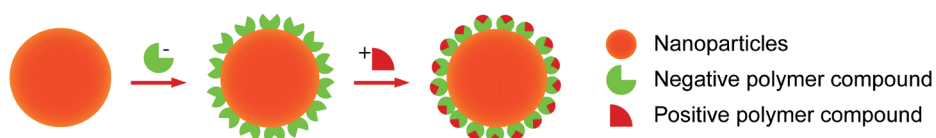


Figure 4 Surface modification methods of RENPs. (a) The ligand oxidation method requires a strong oxidizing agent (Lemieux-von Rudloff reagent, etc.) to oxidize the carbon-carbon double bond to a carboxyl group. (b) The ligand exchange method is used to replace an organic ligand having weak coordination and hydrophobicity with a strong hydrophilic organic ligand. (c) The layer-by-layer self-assembly method relies mainly on the attractive force between oppositely charged molecules, alternately deposits dense monolayers of charged molecules onto oppositely charged surfaces.

3.1 Ligand oxidation

The ligand oxidation method requires a strong oxidizing agent (Lemieux-von Rudloff reagent, etc.) to oxidize the carbon-carbon double bond to a carboxyl group, which is on the surface-coated oleic acid ligand. This reaction can obtain hydrophilic, carboxylic acid-functional RENPs. Thus, the RENPs not only have good water solubility, but also can be directly coupled with diverse biomolecules.

3.2 Ligand exchange

The ligand exchange method is used to replace an organic ligand having weak coordination and hydrophobicity with a strong hydrophilic organic ligand on the surface of the material. This process makes the RENPs hydrophilic and water-soluble.

3.3 Layer-by-layer self-assembly method

The principle of the layer-by-layer self-assembly method[74] is to first wrap a layer of polymer compound with a certain charge on the surface of hydrophobic RENPs. When it is added to a solution of an opposite charged polymer compound, another opposite charged polymer compound can be attracted to the first layer. In this way, the layers are adsorbed, and the upper fluorescent group can be converted, which is possible by alternating self-assembled layers into a polymer layer on the surface of the RENPs. The thickness of the polymer layer can be regulated by changing the number of self-assembled layers so that the RENPs can be stably dispersed in water and have good biocompatibility.

4 Cancer theranostics with NIR-II RENPs

Currently, clinically approved indocyanine green (ICG) and methylene blue (MB) have been used as contrast agents to depict tumor margins in preclinical cancer models and human patients[75-77]. However, these rapidly excreted probes can shorten tumor retention time, affect the process of cancer treatment. On the other hand, due to the renal filtration threshold of ~ 40 kD, most fluorescent probes accumulate largely in the organs of reticuloendothelial system (RES), such as the liver and spleen, leading to long-term safety concerns. Therefore, NIR-II RENPs probes

with long tumor retention period, high signal-to-background ratio and deep tissue penetration have aroused great interest in investigating their applications for cancer theranostics. To reduce the retention time of nanoparticles in the RES system, excretable NIR-II nanoparticles, RENPs@Lips, have been developed for medical imaging and surgical navigation. Under the guidance of NIR-II imaging, RENPs@Lips showed excellent performance in intraoperative identification of orthotopic tumor vessels and embolization surgery, and could perform excellent sentinel lymph node biopsy (SLNB) in tumor-bearing mice[78]. CXCR-4-targeted functional nanoprobe (fReANC) has been demonstrated to detect up to 10.5 mm of deep-targeted subtissue microlesions in lung metastatic models of breast cancer, providing a reliable platform for the detection of targeted subtissue cancerous lesions[79]. At the same time, Dang *et al.* compared several available LbL NIR-II probes, found that rare-earth-based down-conversion nanoparticles can define vascular and skeletal structures, and were evaluated as diagnostic probes for high-grade serous ovarian cancer with the highest resolution out of all of the probes[54]. NIR-II RENPs, with the least interference from scattering and autofluorescence, seemed to represent a promising tool for photothermal therapy(PTT) and photodynamic therapy (PDT). He *et al.* have designed a unique NaGdF₄: Nd@NaGdF₄@NaGdF₄: Yb, Er@NaGdF₄: Yb@NaNdF₄: Yb (LDNPs-5) structure by attaching Au₂₅ clusters and poly(ethylene glycol) (PEG) molecules on nanostructure. Under 808 nm light irradiation, the special LDNPs can efficiently kill tumor cells *in vitro* and *in vivo* due to a synergistic effect arising from the combination of PTT effect generated from Nd³⁺ with PDT[80]. In addition, a three-layer core-shell-shell nanocomposite (NaYF₄: Nd³⁺@NaLuF₄@PDA₁₈) showed an excellent PTT effect in ablation tumors[81]. Recently, dual-mode SWIR imaging and MRI guided PTT was performed in a nude mouse model by using NaErF₄@NaGdF₄ (Er@Gd), which can effectively be used to ablate tumors and provide a new way for cancer theranostics[82]. NaErF₄@NaYF₄@NaNdF₄@Prussian blue (PB) encapsulated in a phospholipid PEG micelle (PEG-CSS@

PB) has been serve as an efficient theranostic agent for NIRII-image guided PTT. In this study, tumors treated with PTT shrank ~12-fold compared with untreated tumors[83]. To achieve accurate tumor localization and a high cancer therapeutic efficacy, Liu *et al.* developed an ultrasmall pH-responsive photothermal gallic acid-iron complex-modified NaDyF₄: Nd nanoprobe to enhance cancer theranostic by *in situ* aggregation[43]. In addition, a theranostic nanoparticle based on RENPs has been developed for gene therapy. Polyethylenimine (PEI) coated β -NaY_{0.78}F₄:Yb_{0.20},Er_{0.02}@NaYF₄ was designed to deliver genetic cargo in an *in vitro* cancer model and detect tumor lesions in a lung metastases model of breast cancer. This strategy will make it possible to develop a nanotheranostic platform for gene therapy[84]. In summary, NIR-II RENPs have great potential in cancer theranostics.

5 Discussion

Overall, RENPs are promising candidates for NIR-II biomedical imaging due to their low toxicity, high photostability, deep tissue penetration, and tunable pharmacokinetic behavior. Despite these successful gains, challenges still remain in the bioimaging applications of NIR-II RENPs. One of them is the limitation of the emission center, which is the fluorescence core of the RENPs. As we know, five rare earth elements (Nd³⁺, Tm³⁺, Pr³⁺, Ho³⁺, Er³⁺) can be the emission centers in NIR-II RENPs, which are excited by 808 nm or 980 nm lasers. However, the RENPs that have been developed are still mainly based on Nd³⁺ and Er³⁺ as the emission centers, which greatly limits the development and application of near-infrared probe types. Although other rare earth elements have also been presented, such efforts should be devoted to design novel NIR-II RENPs probes. For example, Liu *et al.* used Er³⁺ as a sensitizer and Ho³⁺ as an emitter to make a core-shell structured NaErF₄: Ho@NaYF₄ nanoparticle, which emitted at 1180 nm[34]. Besides that, the size of the RENPs has always been a concern in bioimaging.

Smaller size nanoparticles can effectively enter biological tissues, even cells, but the luminescence intensity of nanomaterials will decrease. Although the commonly used core-shell structure can enhance the luminescence intensity, it will increase the size, making it difficult for the nanoparticles to gain entry into biological tissues and the digestion time will become longer. Designing suitable size nanoparticles is still an essential task to promote the NIR-II bioimaging applications of RENPs. All of these studies in the past decades have pointed out that RENPs will play an important role in drug delivery tracking and multispectral molecular imaging in the near future.

References

- [1] E.H. Rubin, J.D. Allen, J.A. Nowak, S.E. Bates, Developing precision medicine in a global world, *Clinical Cancer Research* 20(6) (2014) 1419-1427.
- [2] M.K. Kuimova, S.W. Botchway, A.W. Parker, M. Balaz, H.A. Collins, H.L. Anderson, K. Suhling, P.R. Ogilby, Imaging intracellular viscosity of a single cell during photoinduced cell death, *Nature chemistry* 1(1) (2009) 69-73.
- [3] R. Weissleder, M.C. Schwaiger, S.S. Gambhir, H. Hricak, Imaging approaches to optimize molecular therapies, *Science translational medicine* 8(355) (2016) 355ps16-355ps16.
- [4] Y. Yang, Y. Chao, J. Liu, Z. Dong, W. He, R. Zhang, K. Yang, M. Chen, Z. Liu, Core-shell and co-doped nanoscale metal-organic particles (NMOPs) obtained via post-synthesis cation exchange for multimodal imaging and synergistic thermo-radiotherapy, *NPG Asia Materials* 9(1) (2017) e344-e344.
- [5] A. Quon, S.S. Gambhir, FDG-PET and beyond: molecular breast cancer imaging, *Journal of clinical oncology* 23(8) (2005) 1664-1673.
- [6] R. Weissleder, M.J. Pittet, Imaging in the era of molecular oncology, *Nature* 452(7187) (2008) 580-589.
- [7] J.K. Willmann, N. Van Bruggen, L.M. Dinkelborg, S.S. Gambhir, Molecular imaging in drug development, *Nature reviews Drug discovery* 7(7) (2008) 591-607.
- [8] R.Y. Tsien, Imagining imaging's future, *Nature reviews. Molecular cell biology* (2003) S16-21.
- [9] G. Mariani, L. Moresco, G. Viale, G. Villa, M. Bagnasco, G. Canavese, J. Buscombe, H.W. Strauss, G. Paganelli, Radioguided sentinel lymph node biopsy in breast cancer surgery, *Journal of Nuclear Medicine* 42(8) (2001)

1198-1215.

[10] G. Mariani, M. Gipponi, L. Moresco, G. Villa, M. Bartolomei, G. Mazzarol, M.C. Bagnara, A. Romanini, F. Cafiero, G. Paganelli, Radioguided sentinel lymph node biopsy in malignant cutaneous melanoma, *Journal of Nuclear Medicine* 43(6) (2002) 811-827.

[11] D.H. O'leary, J.F. Polak, R.A. Kronmal, T.A. Manolio, G.L. Burke, S.K. Wolfson Jr, Carotid-artery intima and media thickness as a risk factor for myocardial infarction and stroke in older adults, *New England Journal of Medicine* 340(1) (1999) 14-22.

[12] J.-F.o. Toussaint, G.M. LaMuraglia, J.F. Southern, V. Fuster, H.L. Kantor, Magnetic resonance images lipid, fibrous, calcified, hemorrhagic, and thrombotic components of human atherosclerosis in vivo, *Circulation* 94(5) (1996) 932-938.

[13] M.J. Paulus, S.S. Gleason, S.J. Kennel, P.R. Hunsicker, D.K. Johnson, High resolution X-ray computed tomography: an emerging tool for small animal cancer research, *Neoplasia* 2(1-2) (2000) 62-70.

[14] Y. Yang, J. Mu, B. Xing, Photoactivated drug delivery and bioimaging, *Wiley Interdisciplinary Reviews: Nanomedicine and Nanobiotechnology* 9(2) (2017) e1408.

[15] Y. Yang, J. Aw, B. Xing, Nanostructures for NIR light-controlled therapies, *Nanoscale* 9(11) (2017) 3698-3718.

[16] Y. Fan, F. Zhang, A new generation of NIR-II probes: lanthanide-based nanocrystals for bioimaging and biosensing, *Advanced Optical Materials* 7(7) (2019) 1801417.

[17] H. Gong, R. Peng, Z. Liu, Carbon nanotubes for biomedical imaging: the recent advances, *Advanced Drug Delivery Reviews* 65(15) (2013) 1951-1963.

- [18] C. Liang, S. Diao, C. Wang, H. Gong, T. Liu, G. Hong, X. Shi, H. Dai, Z. Liu, Tumor metastasis inhibition by imaging-guided photothermal therapy with single-walled carbon nanotubes, *Advanced materials* 26(32) (2014) 5646-5652.
- [19] Z. Lei, C. Sun, P. Pei, S. Wang, D. Li, X. Zhang, F. Zhang, Stable, wavelength-tunable fluorescent dyes in the NIR-II region for in vivo high-contrast bioimaging and multiplexed biosensing, *Angewandte Chemie* 131(24) (2019) 8250-8255.
- [20] S. Wang, Y. Fan, D. Li, C. Sun, Z. Lei, L. Lu, T. Wang, F. Zhang, Anti-Quenching NIR-II Molecular Fluorophores for, *Vivo*, 2019.
- [21] G. Hong, Y. Zou, A.L. Antaris, S. Diao, D. Wu, K. Cheng, X. Zhang, C. Chen, B. Liu, Y. He, Ultrafast fluorescence imaging in vivo with conjugated polymer fluorophores in the second near-infrared window, *Nature communications* 5(1) (2014) 1-9.
- [22] C. Li, Y. Zhang, M. Wang, Y. Zhang, G. Chen, L. Li, D. Wu, Q. Wang, In vivo real-time visualization of tissue blood flow and angiogenesis using Ag₂S quantum dots in the NIR-II window, *Biomaterials* 35(1) (2014) 393-400.
- [23] K. Cai, W. Zhang, M.F. Foda, X. Li, J. Zhang, Y. Zhong, H. Liang, H. Li, H. Han, T. Zhai, Miniature Hollow Gold Nanorods with Enhanced Effect for In Vivo Photoacoustic Imaging in the NIR-II Window, *Small* 16(37) (2020) 2002748.
- [24] T. He, C. Jiang, J. He, Y. Zhang, G. He, J. Wu, J. Lin, X. Zhou, P. Huang, Manganese-Dioxide-Coating-Instructed Plasmonic Modulation of Gold Nanorods for Activatable Duplex-Imaging-Guided NIR-II Photothermal-Chemodynamic Therapy, *Advanced Materials* 33(13) (2021) 2008540.
- [25] S. Wang, L. Liu, Y. Fan, A.M. El-Toni, M.S. Alhoshan, D. Li, F. Zhang, In vivo high-resolution ratiometric fluorescence imaging of inflammation using

NIR-II nanoprobes with 1550 nm emission, *Nano Letters* 19(4) (2019) 2418-2427.

[26] Y. Fan, S. Wang, F. Zhang, Optical multiplexed bioassays for improved biomedical diagnostics, *Angewandte Chemie* 131(38) (2019) 13342-13353.

[27] E. Hemmer, A. Benayas, F. Légaré, F. Vetrone, Exploiting the biological windows: current perspectives on fluorescent bioprobes emitting above 1000 nm, *Nanoscale Horizons* 1(3) (2016) 168-184.

[28] M. Kamimura, T. Matsumoto, S. Suyari, M. Umezawa, K. Soga, Ratiometric near-infrared fluorescence nanothermometry in the OTN-NIR (NIR II/III) biological window based on rare-earth doped β -NaYF₄ nanoparticles, *Journal of Materials Chemistry B* 5(10) (2017) 1917-1925.

[29] U. Rocha, K.U. Kumar, C. Jacinto, I. Villa, F. Sanz-Rodríguez, M. del Carmen Iglesias de la Cruz, A. Juarranz, E. Carrasco, F.C. van Veggel, E. Bovero, Neodymium-Doped LaF₃ Nanoparticles for Fluorescence Bioimaging in the Second Biological Window, *small* 10(6) (2014) 1141-1154.

[30] X. Jiang, C. Cao, W. Feng, F. Li, Nd³⁺-doped LiYF₄ nanocrystals for bioimaging in the second near-infrared window, *Journal of Materials Chemistry B* 4(1) (2016) 87-95.

[31] R. Wang, X. Li, L. Zhou, F. Zhang, Epitaxial seeded growth of rare-earth nanocrystals with efficient 800 nm near-infrared to 1525 nm short-wavelength infrared downconversion photoluminescence for in vivo bioimaging, *Angewandte Chemie International Edition* 53(45) (2014) 12086-12090.

[32] H. Dong, S.-R. Du, X.-Y. Zheng, G.-M. Lyu, L.-D. Sun, L.-D. Li, P.-Z. Zhang, C. Zhang, C.-H. Yan, Lanthanide Nanoparticles: From Design toward Bioimaging and Therapy, *Chemical Reviews* 115(19) (2015) 10725-10815.

[33] H. Zhang, Z.-H. Chen, X. Liu, F. Zhang, A mini-review on recent progress

of new sensitizers for luminescence of lanthanide doped nanomaterials, *Nano Research* 13(7) (2020) 1795-1809.

[34] L. Liu, S. Wang, B. Zhao, P. Pei, Y. Fan, X. Li, F. Zhang, Er³⁺ Sensitized 1530 nm to 1180 nm second near-infrared window upconversion nanocrystals for in vivo biosensing, *Angewandte Chemie* 130(25) (2018) 7640-7644.

[35] T.-M. Liu, J. Conde, T. Lipiński, A. Bednarkiewicz, C.-C. Huang, Revisiting the classification of NIR-absorbing/emitting nanomaterials for in vivo bioapplications, *NPG Asia Materials* 8(8) (2016) e295-e295.

[36] Y.-F. Wang, G.-Y. Liu, L.-D. Sun, J.-W. Xiao, J.-C. Zhou, C.-H. Yan, Nd³⁺-Sensitized Upconversion Nanophosphors: Efficient In Vivo Bioimaging Probes with Minimized Heating Effect, *ACS Nano* 7(8) (2013) 7200-7206.

[37] I. Villa, A. Vedda, I.X. Cantarelli, M. Pedroni, F. Piccinelli, M. Bettinelli, A. Speghini, M. Quintanilla, F. Vetrone, U. Rocha, 1.3 μm emitting SrF₂: Nd³⁺ nanoparticles for high contrast in vivo imaging in the second biological window, *Nano Research* 8(2) (2015) 649-665.

[38] Z.-f. Yu, J.-p. Shi, J.-l. Li, P.-h. Li, H.-w. Zhang, Luminescence enhancement of CaF₂:Nd³⁺ nanoparticles in the second near-infrared window for in vivo imaging through Y³⁺ doping, *Journal of Materials Chemistry B* 6(8) (2018) 1238-1243.

[39] J.W. Stouwdam, F.C. van Veggel, Near-infrared emission of redispersible Er³⁺, Nd³⁺, and Ho³⁺ doped LaF₃ nanoparticles, *Nano letters* 2(7) (2002) 733-737.

[40] F. Wang, Y. Zhang, X. Fan, M. Wang, Facile synthesis of water-soluble LaF₃: Ln³⁺ nanocrystals, *Journal of Materials Chemistry* 16(11) (2006) 1031-1034.

[41] Q. Yang, X. Li, Z. Xue, Y. Li, M. Jiang, S. Zeng, Short-wave near-infrared

emissive GdPO₄: Nd³⁺ theranostic probe for in vivo bioimaging beyond 1300 nm, *RSC advances* 8(23) (2018) 12832-12840.

[42] X. Li, Q. Zhang, Z. Ahmad, J. Huang, Z. Ren, W. Weng, G. Han, C. Mao, Near-infrared luminescent CaTiO₃: Nd³⁺ nanofibers with tunable and trackable drug release kinetics, *Journal of materials chemistry B* 3(37) (2015) 7449-7456.

[43] Y. Liu, H. Fan, Q. Guo, A. Jiang, X. Du, J. Zhou, Ultra-small pH-responsive Nd-doped NaDyF₄ nanoagents for enhanced cancer theranostic by in situ aggregation, *Theranostics* 7(17) (2017) 4217.

[44] X. Zhang, Z. Zhao, X. Zhang, D.B. Cordes, B. Weeks, B. Qiu, K. Madanan, D. Sardar, J. Chaudhuri, Magnetic and optical properties of NaGdF₄: Nd³⁺, Yb³⁺, Tm³⁺ nanocrystals with upconversion/downconversion luminescence from visible to the near-infrared second window, *Nano Research* 8(2) (2015) 636-648.

[45] G. Chen, T.Y. Ohulchanskyy, S. Liu, W.-C. Law, F. Wu, M.T. Swihart, H. Ågren, P.N. Prasad, Core/shell NaGdF₄: Nd³⁺/NaGdF₄ nanocrystals with efficient near-infrared to near-infrared downconversion photoluminescence for bioimaging applications, *ACS nano* 6(4) (2012) 2969-2977.

[46] D.H. Ortgies, M. Tan, E.C. Ximendes, B. Del Rosal, J. Hu, L. Xu, X. Wang, E. Martín Rodríguez, C. Jacinto, N. Fernandez, Lifetime-encoded infrared-emitting nanoparticles for in vivo multiplexed imaging, *ACS nano* 12(5) (2018) 4362-4368.

[47] P. Wang, Y. Fan, L. Lu, L. Liu, L. Fan, M. Zhao, Y. Xie, C. Xu, F. Zhang, NIR-II nanoprobes in-vivo assembly to improve image-guided surgery for metastatic ovarian cancer, *Nature communications* 9(1) (2018) 1-10.

[48] M. Zhao, R. Wang, B. Li, Y. Fan, Y. Wu, X. Zhu, F. Zhang, Precise In Vivo Inflammation Imaging Using In Situ Responsive Cross-linking of Glutathione-

Modified Ultra-Small NIR-II Lanthanide Nanoparticles, *Angewandte Chemie* 131(7) (2019) 2072-2076.

[49] M. Zhao, B. Li, P. Wang, L. Lu, Z. Zhang, L. Liu, S. Wang, D. Li, R. Wang, F. Zhang, Supramolecularly engineered NIR-II and Upconversion nanoparticles in vivo assembly and disassembly to improve bioimaging, *Advanced Materials* 30(52) (2018) 1804982.

[50] S. He, S. Chen, D. Li, Y. Wu, X. Zhang, J. Liu, J. Song, L. Liu, J. Qu, Z. Cheng, High affinity to skeleton rare earth doped nanoparticles for near-infrared II imaging, *Nano Letters* 19(5) (2019) 2985-2992.

[51] M. Kamimura, N. Kanayama, K. Tokuzen, K. Soga, Y. Nagasaki, Near-infrared (1550 nm) in vivo bioimaging based on rare-earth doped ceramic nanophosphors modified with PEG-b-poly (4-vinylbenzylphosphonate), *Nanoscale* 3(9) (2011) 3705-3713.

[52] D. Naczynski, M. Tan, M. Zevon, B. Wall, J. Kohl, A. Kulesa, S. Chen, C. Roth, R. Riman, P. Moghe, Rare-earth-doped biological composites as in vivo shortwave infrared reporters, *Nature communications* 4(1) (2013) 1-10.

[53] Z. Xue, S. Zeng, J. Hao, Non-invasive through-skull brain vascular imaging and small tumor diagnosis based on NIR-II emissive lanthanide nanoprobe beyond 1500 nm, *Biomaterials* 171 (2018) 153-163.

[54] X. Dang, L. Gu, J. Qi, S. Correa, G. Zhang, A.M. Belcher, P.T. Hammond, Layer-by-layer assembled fluorescent probes in the second near-infrared window for systemic delivery and detection of ovarian cancer, *Proceedings of the National Academy of Sciences* 113(19) (2016) 5179-5184.

[55] H. Kantamneni, M. Zevon, M.J. Donzanti, X. Zhao, Y. Sheng, S.R. Barkund, L.H. McCabe, W. Banach-Petrosky, L.M. Higgins, S. Ganesan, Surveillance nanotechnology for multi-organ cancer metastases, *Nature biomedical engineering* 1(12) (2017) 993-1003.

- [56] Z. Deng, X. Li, Z. Xue, M. Jiang, Y. Li, S. Zeng, H. Liu, A high performance Sc-based nanoprobe for through-skull fluorescence imaging of brain vessels beyond 1500 nm, *Nanoscale* 10(19) (2018) 9393-9400.
- [57] Y. Zhong, Z. Ma, S. Zhu, J. Yue, M. Zhang, A.L. Antaris, J. Yuan, R. Cui, H. Wan, Y. Zhou, Boosting the down-shifting luminescence of rare-earth nanocrystals for biological imaging beyond 1500 nm, *Nature communications* 8(1) (2017) 1-7.
- [58] X. Lei, R. Li, D. Tu, X. Shang, Y. Liu, W. You, C. Sun, F. Zhang, X. Chen, Intense near-infrared-II luminescence from NaCeF₄: Er/Yb nanoprobes for in vitro bioassay and in vivo bioimaging, *Chemical science* 9(20) (2018) 4682-4688.
- [59] H. Zhang, Y. Fan, P. Pei, C. Sun, L. Lu, F. Zhang, Tm³⁺-Sensitized NIR-II Fluorescent Nanocrystals for In Vivo Information Storage and Decoding, *Angewandte Chemie International Edition* 58(30) (2019) 10153-10157.
- [60] Y. Fan, P. Wang, Y. Lu, R. Wang, L. Zhou, X. Zheng, X. Li, J.A. Piper, F. Zhang, Lifetime-engineered NIR-II nanoparticles unlock multiplexed in vivo imaging, *Nature nanotechnology* 13(10) (2018) 941-946.
- [61] D. Wang, D. Wang, A. Kuzmin, A. Pliss, W. Shao, J. Xia, J. Qu, P.N. Prasad, ICG-Sensitized NaYF₄: Er Nanostructure for Theranostics, *Advanced Optical Materials* 6(12) (2018) 1701142.
- [62] X. Li, M. Jiang, S. Zeng, H. Liu, Polydopamine coated multifunctional lanthanide theranostic agent for vascular malformation and tumor vessel imaging beyond 1500 nm and imaging-guided photothermal therapy, *Theranostics* 9(13) (2019) 3866.
- [63] M.C. Tan, D.J. Naczynski, P.V. Moghe, R.E. Riman, Engineering the design of brightly-emitting luminescent nanostructured photonic composite systems, *Australian Journal of Chemistry* 66(9) (2013) 1008-1020.

- [64] Q. Wang, M.C. Tan, R. Zhuo, G. Kumar, R.E. Riman, A solvothermal route to size-and phase-controlled highly luminescent NaYF₄: Yb, Er up-conversion nanocrystals, *Journal of nanoscience and nanotechnology* 10(3) (2010) 1685-1692.
- [65] M.C. Tan, G. Kumar, R.E. Riman, M. Brik, E. Brown, U. Hommerich, Synthesis and optical properties of infrared-emitting YF₃: Nd nanoparticles, *Journal of Applied Physics* 106(6) (2009) 063118.
- [66] D. Yuan, M.C. Tan, R.E. Riman, G.M. Chow, Comprehensive study on the size effects of the optical properties of NaYF₄: Yb, Er nanocrystals, *The Journal of Physical Chemistry C* 117(25) (2013) 13297-13304.
- [67] H.-X. Mai, Y.-W. Zhang, L.-D. Sun, C.-H. Yan, Size-and phase-controlled synthesis of monodisperse NaYF₄: Yb, Er nanocrystals from a unique delayed nucleation pathway monitored with upconversion spectroscopy, *The Journal of Physical Chemistry C* 111(37) (2007) 13730-13739.
- [68] F. Zhang, Y. Wan, T. Yu, F. Zhang, Y. Shi, S. Xie, Y. Li, L. Xu, B. Tu, D. Zhao, Uniform nanostructured arrays of sodium rare-earth fluorides for highly efficient multicolor upconversion luminescence, *Angewandte Chemie* 119(42) (2007) 8122-8125.
- [69] X. Li, D. Shen, J. Yang, C. Yao, R. Che, F. Zhang, D. Zhao, Successive layer-by-layer strategy for multi-shell epitaxial growth: shell thickness and doping position dependence in upconverting optical properties, *Chemistry of Materials* 25(1) (2013) 106-112.
- [70] X. Li, R. Wang, F. Zhang, D. Zhao, Engineering homogeneous doping in single nanoparticle to enhance upconversion efficiency, *Nano letters* 14(6) (2014) 3634-3639.
- [71] A. Dong, X. Ye, J. Chen, Y. Kang, T. Gordon, J.M. Kikkawa, C.B. Murray, A generalized ligand-exchange strategy enabling sequential surface

functionalization of colloidal nanocrystals, *Journal of the American Chemical Society* 133(4) (2011) 998-1006.

[72] F. Wang, X. Liu, Recent advances in the chemistry of lanthanide-doped upconversion nanocrystals, *Chemical Society Reviews* 38(4) (2009) 976-989.

[73] C. Li, J. Lin, Rare earth fluoride nano-/microcrystals: synthesis, surface modification and application, *Journal of Materials Chemistry* 20(33) (2010) 6831-6847.

[74] D. Wang, A. Rogach, F. Caruso, Nanocrystal-labeled biofunctional colloids, *Nano Lett* 2(857) (2002) 10.1021.

[75] H. Wang, P. Agarwal, S. Zhao, J. Yu, X. Lu, X. He, A biomimetic hybrid nanoplatform for encapsulation and precisely controlled delivery of theranostic agents, *Nature communications* 6(1) (2015) 1-13.

[76] J.H. Winer, H.S. Choi, S.L. Gibbs-Strauss, Y. Ashitate, Y.L. Colson, J.V. Frangioni, Intraoperative localization of insulinoma and normal pancreas using invisible near-infrared fluorescent light, *Annals of surgical oncology* 17(4) (2010) 1094-1100.

[77] A.L. Vahrmeijer, M. Hutteman, J.R. Van Der Vorst, C.J. Van De Velde, J.V. Frangioni, Image-guided cancer surgery using near-infrared fluorescence, *Nature reviews Clinical oncology* 10(9) (2013) 507-518.

[78] D. Li, S. He, Y. Wu, J. Liu, Q. Liu, B. Chang, Q. Zhang, Z. Xiang, Y. Yuan, C. Jian, Excretable lanthanide nanoparticle for biomedical imaging and surgical navigation in the second near-infrared window, *Advanced Science* 6(23) (2019) 1902042.

[79] M. Zevon, V. Ganapathy, H. Kantamneni, M. Mingozi, P. Kim, D. Adler, Y. Sheng, M.C. Tan, M. Pierce, R.E. Riman, CXCR-4 targeted, short wave infrared (SWIR) emitting nanoprobe for enhanced deep tissue imaging and micrometastatic cancer lesion detection, *Small* 11(47) (2015) 6347-6357.

[80] F. He, L. Feng, P. Yang, B. Liu, S. Gai, G. Yang, Y. Dai, J. Lin, Enhanced up/down-conversion luminescence and heat: simultaneously achieving in one single core-shell structure for multimodal imaging guided therapy, *Biomaterials* 105 (2016) 77-88.

[81] Y. Dai, D. Yang, D. Yu, C. Cao, Q. Wang, S. Xie, L. Shen, W. Feng, F. Li, Mussel-inspired polydopamine-coated lanthanide nanoparticles for NIR-II/CT dual imaging and photothermal therapy, *ACS Applied Materials & Interfaces* 9(32) (2017) 26674-26683.

[82] L. Ma, Y. Liu, L. Liu, A. Jiang, F. Mao, D. Liu, L. Wang, J. Zhou, Simultaneous activation of short-wave infrared (SWIR) light and paramagnetism by a functionalized shell for high penetration and spatial resolution theranostics, *Advanced Functional Materials* 28(6) (2018) 1705057.

[83] X. Wang, H. Li, F. Li, X. Han, G. Chen, Prussian blue-coated lanthanide-doped core/shell/shell nanocrystals for NIR-II image-guided photothermal therapy, *Nanoscale* 11(45) (2019) 22079-22088.

[84] Z. Zhao, H. Kantamneni, S. He, S. Pelka, A.S. Venkataraman, M. Kwon, S.K. Libutti, M. Pierce, P.V. Moghe, V. Ganapathy, Surface-modified shortwave-infrared-emitting nanophotonic reporters for gene-therapy applications, *ACS biomaterials science & engineering* 4(7) (2018) 2350-2363.

